Investigation on the adsorption kinetics and diffusion of methane in shale samples

Jie Zou [a], Reza Rezaee [a], Yujie Yuan[a]

[a] *Department of Petroleum Engineering, Curtin University, Perth, 6151, Australia*

Abstract

Shale gas is becoming increasingly important to mitigate the energy crisis of the world. Understanding the mechanisms of gas transport in shale matrix is crucial for development strategies. In this study, methane adsorption kinetics in shale samples were measured under different pressures and temperatures. The results of methane adsorption rate were fitted by the bidisperse diffusion model. Pore structure of the shale samples were characterized by low-pressure N_2 and CO_2 adsorption. The results showed that pressure has a negative effect on methane adsorption rate and diffusion, while the effect of temperature is positive. Combining the total organic carbon (TOC) and pore structure, methane adsorption rate and effective diffusivity were compared between all the shale samples. The methane adsorption rate under high pressure (50bar) is positively related to the TOC content. The micropore volume showed a moderate positive relation with the methane adsorption rate at 30bar. A weak positive relation exists between the TOC and effective diffusivity at low pressure and the effective diffusivity at low pressure shows an increasing trend with micropore(<2nm) volume. A hypothetic pore model is proposed: micropore in shales controls gas diffusion as pore throat which connects pores.

Keywords: shale gas, adsorption rate, diffusion, bidisperse model, methane

1. Introduction

With the consumption of the fossil fuels increasing rapidly, shale gas has drawn much attention as unconventional natural gas all over the world. However, the mechanisms of gas storage and transport in shale differ significantly from conventional gas reservoirs. Shale consists of both organic and inorganic matter, with complex and heterogeneous geological properties (Bustin and Bustin, 2012; Liu et al., 2017). Moreover, shale gas is stored not only as free gas in pores, but also as adsorbed gas on pore surface and dissolved gas in organic matter such as bitumen (Chalmers and Bustin, 2007; Curtis, 2002; Ross and Marc Bustin, 2007). These specific features make it impossible to directly apply knowledge of conventional gas reservoirs for shale. Considering that the percentage of the adsorbed gas could be significant, the contribution of the adsorbed gas to the gas storage and transport in shale is a very important subject.

With respect to gas storage in shale, gas adsorption capacity has been well documented on its controlling factors, including reservoir conditions (pressure, temperature and moisture) and shale properties (organic matter content, clay mineral content and pore structure) (Chalmers and Bustin, 2010; Guo, 2013; Ji et al., 2012; Ross and Marc Bustin, 2009; Wang and Yu, 2016; Zhang et al., 2012). With respect to gas transport in shale, the mechanisms related to the adsorbed gas include the gas adsorption, desorption, diffusion and Darcy flow. Given that a large proportion of pores in shale are nano-scale (Kuila et al., 2014; Labani et al., 2013), gas flow in nano-scale pores is mainly limited by the gas diffusion rather than the Darcy flow(CUI et al., 2009), which occurs in big pores or factures. Therefore, the adsorption kinetics from

methane adsorption experiments describe the process of gas diffusion in pore throats and gas adsorption on pore surfaces (Wang et al., 2016).

Some scholars have realised the importance of gas adsorption kinetics in coal and shale (Bhowmik and Dutta, 2013; Gasparik et al., 2014; Mianowski and Marecka, 2009). Methane adsorption rate data has been analysed for shale samples, showing a negative relation between the adsorption rate and pressure (Dang et al., 2017; Wang et al., 2016). In addition, the diffusion behaviour in porous material can be indirectly obtained from adsorption kinetics using diffusion models, such as the "unipore diffusion model" and the "bidisperse diffusion model". Even though the unipore diffusion model has been successfully used for high rank coals (Clarkson and Bustin, 1999), it is inadequate for shale with heterogeneous pore structures and would overrate the diffusivity (Dang et al., 2017; Yuan et al., 2014). This is because the unipore model assumes that the pore structure is homogenous. Unlike the unipore model, the bidisperse diffusion model was developed for small and large pores in matrix, named as micropore and macropore, respectively (Ruckenstein et al., 1971). Note that the macropore and micropore in the bidisperse model represent pores with different sizes but not any specific sizes. The assumption of the bidisperse model is linear isotherm. The methane adsorption isotherm of low pressure (<4MPa) was observed as linear in shale, and the adsorption rate of low pressure (<4MPa) were well fitted by the bidisperse model in previous work (Yuan et al., 2014). The fitting results have shown that macropore diffusivity decreases with increasing pressure, and both macropore and micropore diffusivity are reduced by water (Yuan et al., 2014). Although some scholars have analysed the gas adsorption rate and applied different diffusion models in shale (Chen et al., 2018; Dang et al., 2017; Rani et al., 2018), details of the gas adsorption kinetics and diffusion in shale are not well understood. In particular, the behavior of gas adsorption kinetics and diffusion in different shale samples are unclear.

In this work, we investigated the adsorption kinetics on different shale samples at ranged temperature and pressure. The gas diffusion parameters were determined by fitting the adsorption rate with the bidisperse diffusion model. The proposed method offers an alternative to the gas desorption measurement for the gas flow parameters in shale if the desorption data is not available. In addition, the analysis of adsorption rate can also give an insight into the process of gas adsorption.

2. Experiment methods

2.1 samples

A total of 5 shale samples from one borehole in the Perth Basin, Western Australia were analysed in this work. The shale samples were chosen with ranged TOC (0.23 to 3.03 wt%) and clay content (28 to 56%) to explore the gas adsorption kinetics on different shale samples. Even though the utilized samples with low TOC are not good quality as shale, the samples were chosen for the wide variation in TOC to investigate the effect of organic matter richness on gas adsorption kinetics and diffusion in shales. Table 1 and 2 show the mineralogical composition and geochemical analysis, respectively.

Table 1 Mineralogical composition for the shale samples studied(Zou et al., 2017)

Sample	Quartz (%)	Smectite (%)	Mixed illite/smectite (20%S)	Illite+mica (%)	Kaolinite (%)	Chlorite (%)	Total Clay (%)	Carbonates (%)
AC3-1	24.5	1.7	19.8	24.9	2.6	7.1	56	4.8
AC3-2	53.0	1.6	11.7	13.9	0.8	3.1	31.1	2.1
AC3-3	41.3	0.9	14.9	18.9	0.8	5.2	40.7	2.8
AC3-4	53.8	1.7	10.4	12.4	0.5	2.9	27.9	4.6
AC3-5	44.5	1.9	9.7	16.0	1.2	4.3	33.1	6.5

Table 2 Geochemical analysis for the shale samples studied(Zou et al., 2017)

Sample	TOC (wt %)	S_1 (mg/g)	S_2 (mg/g)	S_3 (mg/g)	HI	OI	PI	T_{max} °C
AC3-1	3.03	0.54	1.95	0.16	64	5	0.22	459
AC3-2	0.64	0.13	0.25	0.17	39	27	0.34	458
AC3-3	1.82	0.33	1.15	0.03	63	2	0.22	460
AC3-4	1.08	0.19	0.52	0.09	48	8	0.27	465
AC3-5	0.23	0.04	0.10	0.19	43	83	0.29	N/A

Note: T_{max} of sample AC3-5 is not available as the TOC is too low to measure

2.2 Sample preparation

All the samples were crushed into powder and sieved with particle size less than 250 μm for adsorption measurements. The samples were moisturized in a certain relative humidity due to the existing of moisture in actual reservoir condition. According to the American Society for Testing and Materials (ASTM) procedure, the samples were placed into a desiccator with a saturated solution (KCl) at room temperature (25°C) for 72 hours, which can provide a relativity humidity of 84% (Greenspan, 1977).

2.3 Low-pressure N_2 and CO_2 adsorption analysis

Low-pressure N_2 and CO_2 adsorption were measured to characterize the pore structure of the shale samples. Low-pressure N_2 and CO_2 adsorption were conducted at 77K and 273K, respectively. The relative equilibrium adsorption pressure (P/P_0) ranges from 0.01 to 0.99, where P is the gas vapor pressure in the system and P_0 is the saturation pressure.

BET surface area can be obtained from the low-pressure N_2 adsorption by Brunauer-Emmett-Teller method (Brunauer et al., 1938), which is determined in the P/P_0 range of 0.1 to 0.3. The low-pressure N_2 adsorption isotherm can be also interpreted by the density functional theory model (Ravikovitch et al., 1998), which could provide the volume of pore in the range (pore diameter) of 2-100nm. Based on the pore classification proposed by the International Union of Applied and Pure Chemistry (IUPAC), micropores are <2 nm in diameter, mesopores 2-50 nm and macropores >50 nm.(Rouquerol et al., 1994) The CO_2-based adsorption provides the micropore volume by Dubinin-Astakhov (D-A) model (Siemieniewska et al., 1990), which was calculated in the (P/P_0) range of 0.01-0.05. Table 3 shows the pore structure parameters from the low-pressure adsorption. The TOC of sample AC3-1 is 10 times more than that of sample AC3-5, while their BET surface areas are 6.7 and 5.2m2/g, respectively. It is likely that the relationship between TOC and BET surface area is weak and the BET surface area is controlled by various parameters in shales.

Table 3 BET surface area and micropore volume from low-pressure adsorption for the shale samples studied

	BET surface area (m^2/g)	Sum of mesopore and macropore (<100nm) volume ($cm^3/100g$)	Micropore volume ($cm^3/100g$)
AC3-1	6.7	1.598	0.191
AC3-2	3.3	0.462	0.190
AC3-3	7.6	0.958	0.192
AC3-4	4.7	1.138	0.157
AC3-5	5.2	1.331	0.136

2.4 Adsorption rate analysis

Methane adsorption experiments were conducted on Micrometritics high-pressure volumetric analyzer (HPVAII-200). The detailed experiment set up has been documented in our previous study.(Zou et al., 2017) Methane adsorption rate was measured to a maximum pressure of 50bar with a pressure step of 10bar. During each pressure step, pressure (every 0.002bar) in sample cell as a function of time was recorded until meeting the determined equilibrium criteria (pressure variation less than 0.003 bar in one minute or waiting for 60 minutes after dosing the gas into the reference cell). The adsorption rate at any time t can be obtained by the approximation (Busch et al., 2004):

$$M_t/M_\infty \approx (P_0 - P_t)/(P_0 - P_\infty) \qquad \textit{Equation 1}$$

Where, M_t/M_∞ is the ratio of the volume of adsorbed gas at time t and at equilibrium; P_t and P_∞ are the pressure in sample cell at time t and at equilibrium respectively; P_0 is the first pressure in the pressure decay during the adsorption process. Some scholars have mentioned that the pressure increases in a few seconds to attain thermal equilibrium after opening valve and allowing the gas into the sample cell from manifold (Clarkson and Bustin, 1999). Therefore, the maximum pressure at each pressure step was regarded as P_0 . Furthermore, the temperature in manifold was set to be consistent with experiment temperature in sample cell. The experiment temperature was 25°C for all samples, and sample AC3-1 with the highest TOC (3.03%) and sample AC 3-5 with the lowest TOC (0.23%) were also measured at 45 and 60°C.

2.5 Bidisperse diffusion model

The bidisperse diffusion model describes the gas diffusion in a spherical particle comprising an agglomeration of small pores within a large pore (Ruckenstein et al., 1971). The small pore and large pore are regarded as micropore and macropore, respectively. The equations of gas diffusion in micropore and macropore are provided as following(Ruckenstein et al., 1971):

$$\frac{D_a\varepsilon_a}{{r_a}^2}\frac{\partial}{\partial r_a}\left[{r_a}^2\frac{\partial C_a}{\partial r_a}\right]=\varepsilon_a\frac{\partial C_a}{\partial t}+S_a\frac{\partial C_{sa}}{\partial t}+n4\pi{R_i}^2\varepsilon_i D_i\left(\frac{\partial C_i}{\partial r_i}\right)_{r_i=R_i} \quad \textit{Equation 2}$$

$$\frac{D_i\varepsilon_i}{{r_i}^2}\frac{\partial}{\partial r_i}\left[{r_i}^2\frac{\partial C_i}{\partial r_i}\right]=\varepsilon_i\frac{\partial C_i}{\partial t}+S_i\frac{\partial C_{si}}{\partial t} \quad \textit{Equation 3}$$

The solutions of the equation 2 and 3 have been given based on the assumption of the linear isotherm. Moreover, a simplified solution has also been provided to easily fit the adsorption rate data.

$$\frac{M_t}{M_\infty}=\frac{\left[1-\frac{6}{\pi^2}\sum_{n=1}^{\infty}\frac{1}{n^2}exp\left(-\frac{n^2\pi^2D_a't}{R_a^2}\right)\right]+\frac{\beta}{3\alpha}\left[1-\frac{6}{\pi^2}\sum_{n=1}^{\infty}\frac{1}{n^2}exp\left(-\frac{n^2\pi^2\alpha D_i't}{R_i^2}\right)\right]}{1+\frac{\beta}{3\alpha}} \quad \textit{Equation 4}$$

Where $=\left.\frac{D_i'}{R_i^2}\right/\frac{D_a'}{R_a^2}$; $D_a'=\frac{D_a}{1+H_aS_a/\varepsilon_a}$; $D_i'=\frac{D_i}{1+H_iS_i/\varepsilon_i}$; $\beta=\frac{3(1-\varepsilon_a)\varepsilon_i}{\varepsilon_a}\frac{R_a^2}{R_i^2}\frac{D_i}{D_a}$.

Where D_a is the macropore diffusivity, m^2/s, D_i is the micropore diffusivity, m^2/s; ε_a is the macropore porosity, ε_i is the micropore porosity; r_a is the distance from macrosphere centre, m, r_i is the distance from microsphere centre, m; C_a is the macropore gas concentration, mol/m^3, C_i is the micropore gas concentration, mol/m^3; C_{sa} is the macropore adsorbed gas concentration, mol/m^2, C_{si} is the micropore adsorbed gas concentration, mol/m^2; H_a is the isotherm constant for macropore, m^3/m^2, H_i is the isotherm constant for micropore, m^3/m^2; S_a is the macropore surface area, m^2/m^3, S_i is the micropore surface area, m^2/m^3; R_i is the microsphere radius, m; R_a is the macrosphere radius, m; n is the number of microspheres per unit volume of macrosphere.

The parameters in the equations, including $\frac{D_a'}{R_a^2}$ and $\frac{D_i'}{R_i^2}$ and $\frac{\beta}{\alpha}$ can be determined by fitting the adsorption rate data from experiment.

3. Results and discussion

3.1 Methane adsorption rate

Figure 1 shows the curves of methane adsorption rate for all the samples at three pressure steps. The three pressure steps were chosen to improve the comparative results, as the curves of adsorption rate under close pressures are similar. For all the curves of methane adsorption rate, the fractional uptake ($\frac{M_t}{M_\infty}$) increases strikingly at the initial time range and then becomes relatively stable in the later period.

3.1.1 Pressure effect on methane adsorption rate

In terms of each shale sample, methane adsorption rate shows a decrease trend with increasing pressure. As shown in Figure 1, adsorption rate at low pressure is larger than that of high pressure. The negative relation between methane adsorption rate and pressure in shale has been observed in previous works (Dang et al., 2017; Rani et al., 2018; Yuan et al., 2014). The phenomenon has been explained that gas molecule-molecule collision is intensive at high pressure, which could lead to a slow gas adsorption (Rani et al., 2018). In addition, according to the pore-filling theory, gas first adsorbs in small pores and then move into bigger pores with increasing pressure. As the adsorption rate at low pressure is greater, it can be suggested that the methane adsorption process in small pores is faster than in large pores.

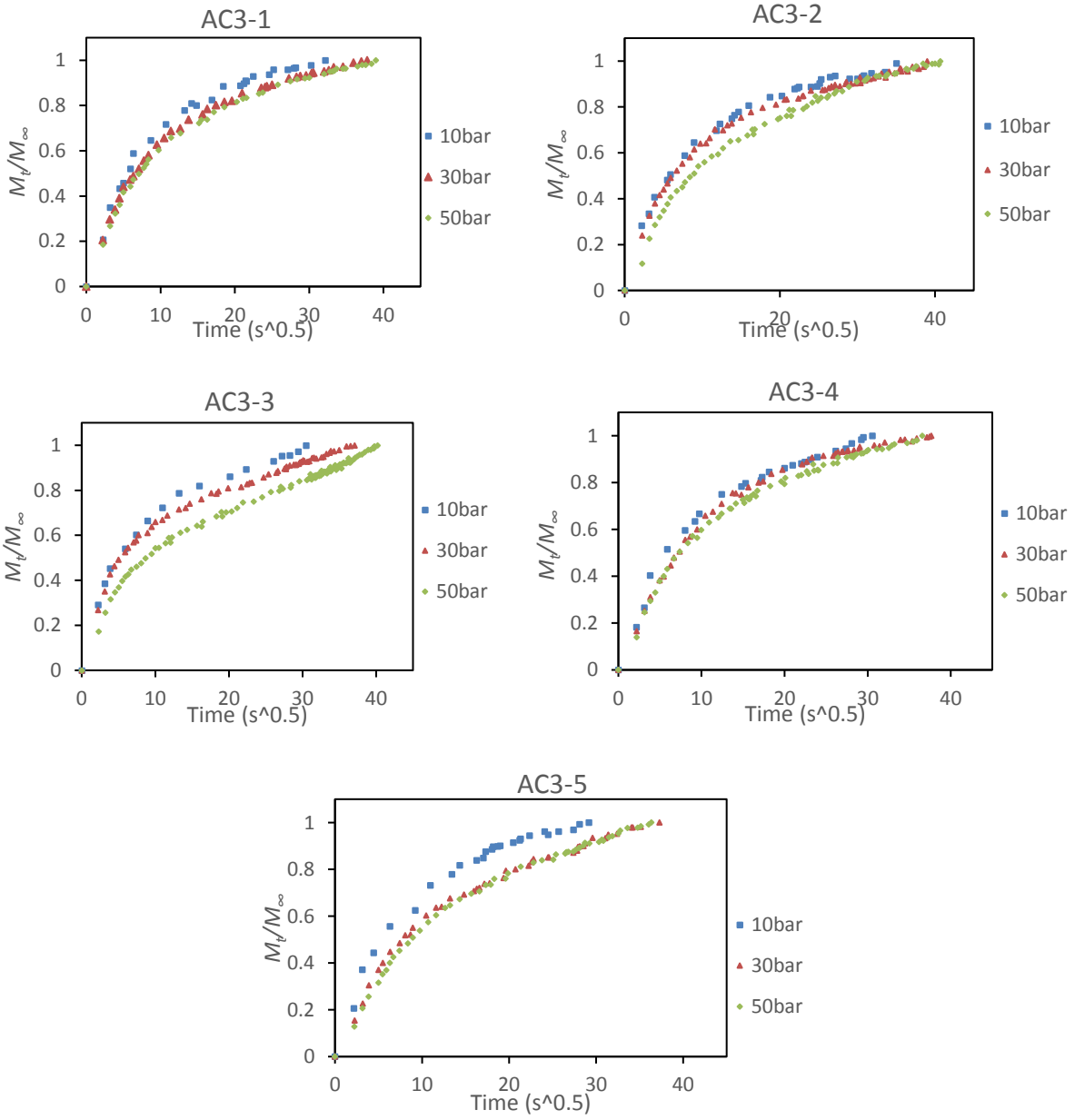

Figure 1 Methane adsorption rate at three pressure steps for the shale samples. The vertical axis is the fraction uptake and the horizontal axis is time in $s^{0.5}$.

3.1.2 Temperature effect on methane adsorption rate

Figure 2 shows the methane adsorption rate at different temperatures for sample AC3-1 and AC3-5. The methane adsorption rate (30bar) is greater at higher temperature, indicating the positive effect of temperature on the methane adsorption rate. It has been explained that gas molecules move faster in pore throats and have more collisions with the pore walls at high temperature, leading to a faster gas transport and adsorption (Wang et al., 2016).

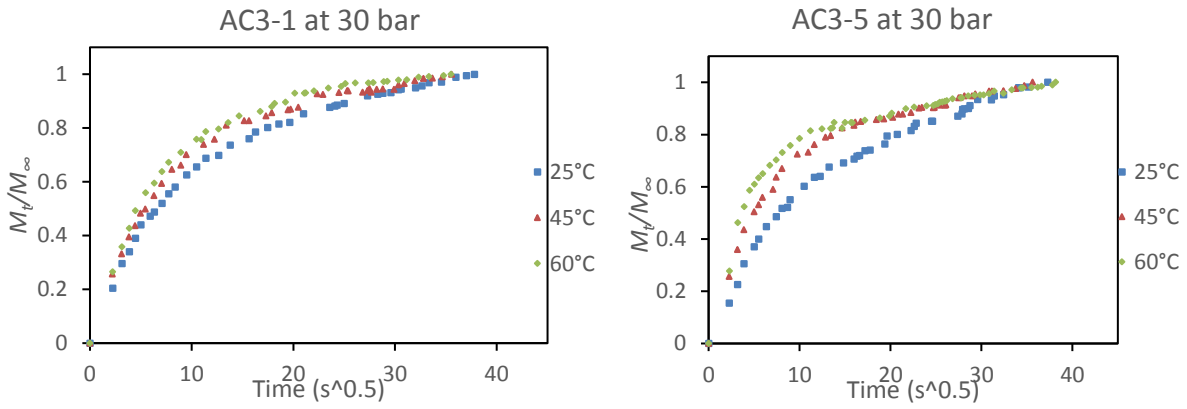

Figure 2 Methane adsorption rate under 30bar at three different temperatures for sample AC3-1 and AC3-5.

3.1.3 Comparison of methane adsorption rate between samples

We also compared the methane adsorption rate of different shale samples at the three pressure steps (10, 30 and 50bar). As the adsorption rate curves are very similar to each other, a quantifying method was used to calculate the slope of the curve in the initial time range, which is regarded as the linear portion of the adsorption rate curve. The time range chosen includes at least 4 time points above zero, so $6s^{0.5}$ was used in each determination of adsorption rate. Table 4 shows the slope of methane adsorption rate at 3 pressure steps for all the samples.

Figure 3 shows a good relation between the TOC and slope of adsorption rate at 50bar, which indicates the organic matter contributes to the methane adsorption rate at high pressure. As for low pressure, the slope of adsorption rate at 10 and 30bar have no relation with the TOC. However, it can be seen in Figure 3 that a moderate positive relation exists between the slop of adsorption rate at 30bar and micropore volume. It might be inferred that the sample with high micropore volume provides more surface area for adsorption and more throat for gas flow, which could lead to a great adsorption rate. Furthermore, the relations between the micropore volume and the slopes of adsorption rate at 10 and 50bar are weak, indicating the effect of micropore volume on adsorption rate is not consistent for different pressure steps. In addition, no relation exists between the sum of mesopore and macropore (<100nm) volume and adsorption rate at the three pressure steps. In a word, the controlling factors of methane adsorption rate is complex, and more parameters need to be studied.

Table 4 The slope of adsorption rate at three pressures for the shale samples

	Slope, 10bar	Slope, 30bar	Slope 50bar
AC3-1	0.093	0.086	0.08
AC3-2	0.094	0.089	0.069
AC3-3	0.105	0.1	0.074
AC3-4	0.091	0.076	0.074
AC3-5	0.091	0.074	0.064

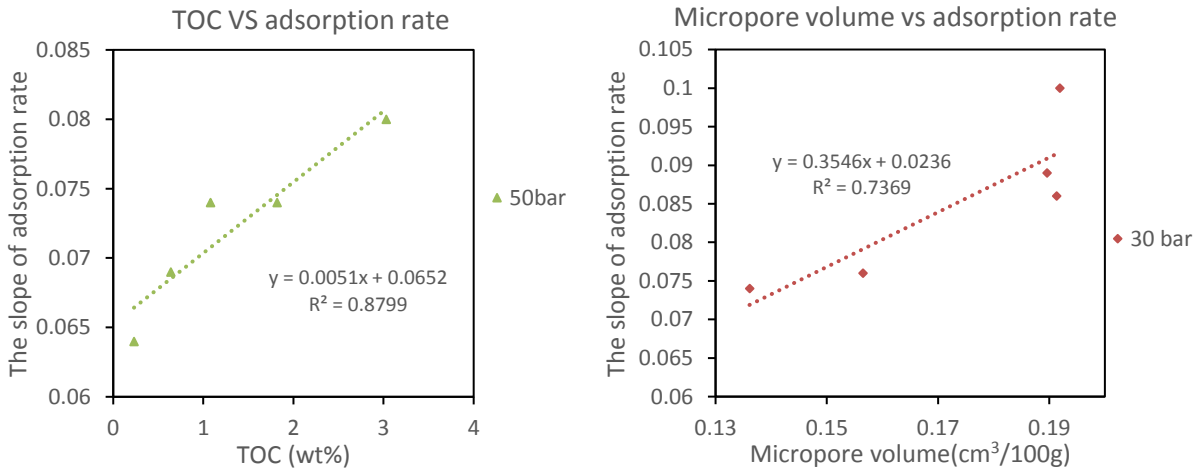

Figure 3 The relation of methane adsorption rate to TOC and micropore volume. TOC shows a good correlation with the slope of adsorption rate at 50bar; a moderate correlation exists between the micropore volume and slope of adsorption rate at 30bar.

4. Diffusivity

The bidisperse diffusion model was used to fit the methane adsorption rate for the shale samples (Figure 4). As shown, the bidisperse diffusion model gives a good matching with the data of methane adsorption rate in shales. The fitting results provide the parameters of the bidisperse diffusion model in table 5 and 6, including $\frac{D_a'}{R_a^2}$ and $\frac{D_i'}{R_i^2}$. R_a, the macrosphere radius, could represent the mean particle radius of sample. As samples were crushed into the same particle size, R_a is consistent for all the samples. As for R_i, it is believed that the microsphere radius (R_i) is controlled by organic matter or clay minerals in shale. Herein, the shale samples are from the same formation of one borehole, so R_i is considered uniform for all the samples. Therefore, informative comparisons on effective diffusivities ($D_a'$and D_i') can be obtained from $\frac{D_a'}{R_a^2}$ and $\frac{D_i'}{R_i^2}$. Table 5 and 6 show that $\frac{D_a'}{R_a^2}$ is larger than $\frac{D_i'}{R_i^2}$ for all the measurements, indicating that the macropore effective diffusivity (D_a') is much greater than the micropore effective diffusivity (D_i'), because the R_i is significantly smaller than the R_a. Therefore, gas diffusion in shale includes a faster macropore diffusion and a slower micropore diffusion.

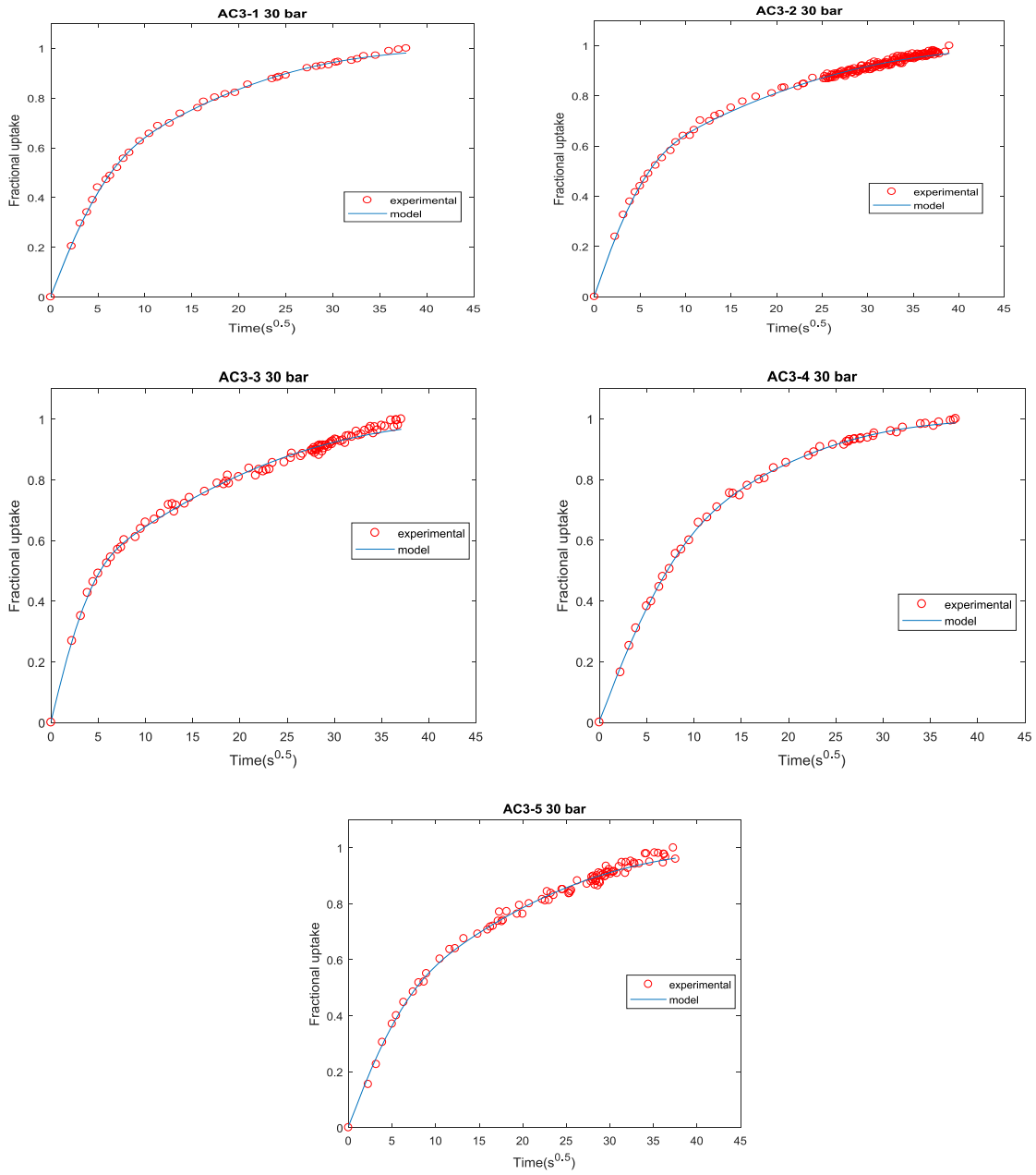

Figure 4 The methane adsorption rate at 30bar fitted using the bidisperse diffusion model for the shale samples.

Both $\frac{D_a{}'}{R_a^2}$ and $\frac{D_i{}'}{R_i^2}$ show a decrease trend with pressure except for the 40bar of sample AC3-1 and AC 3-3 (Table 5). For these two samples, the determined $\frac{D_a{}'}{R_a^2}$ at the pressure step of 40bar is larger than that at 30bar, which was also reported in the previous work (Cui et al., 2004; Dang et al., 2017). The decrease trend suggests a negative pressure effect on the macropore and micropore diffusivity. It has been explained that shale matrix could swell due to methane adsorption. The swelling narrows the pore throat and reduces the permeability (Rani et al., 2018). Even if no swelling exists in shale matrix, the increased adsorbed gas content with increasing pressure could tighten the path for gas transport as well (Li et al., 2016).

Table 6 displays that the $\frac{D_a{}'}{R_a^2}$ increases with increasing temperature for sample AC3-1 and AC3-5, while the $\frac{D_i{}'}{R_i^2}$ shows no obvious trend with increasing temperature, indicating limited temperature effect on the micropore effective diffusivity.

Table 5 Gas diffusion parameters from the bidisperse model for the shale samples at 25°C

	AC3-1M(25°C)		AC3-2M(25°C)		AC3-3M(25°C)	
pressure(bar)	$\frac{D_a{}'}{R_a^2}$	$\frac{D_i{}'}{R_i^2}$	$\frac{D_a{}'}{R_a^2}$	$\frac{D_i{}'}{R_i^2}$	$\frac{D_a{}'}{R_a^2}$	$\frac{D_i{}'}{R_i^2}$
10	0.006234	0.001154	0.005723	0.001226	0.006779	0.001255
20	0.003284	0.000928	0.004171	0.000845	0.00509	0.001143
30	0.003099	0.00091	0.004159	0.000702	0.003404	0.000765
40	0.003381	0.000848	0.003036	0.000716	0.003756	0.00074
50	0.002972	0.000722	0.003128	0.000662	0.003288	0.000625

	AC3-4(25°C)		AC3-5(25°C)	
	$\frac{D_a{}'}{R_a^2}$	$\frac{D_i{}'}{R_i^2}$	$\frac{D_a{}'}{R_a^2}$	$\frac{D_i{}'}{R_i^2}$
10	0.006766	0.002214	0.004371	0.001226
20	0.004035	0.001352	0.003436	0.000845
30	0.003936	0.001093	0.002837	0.000702
40	0.004309	0.000843	0.002246	0.000716
50	0.003848	0.000647	0.002265	0.000662

Table 6 Gas diffusion parameter from bidisperse model for sample AC3-1 and AC3-5 at 45 and 60°C

	AC3-1M(45°C)		AC3-1(60°C)	
pressure(bar)	$\frac{D_a{}'}{R_a^2}$	$\frac{D_i{}'}{R_i^2}$	$\frac{D_a{}'}{R_a^2}$	$\frac{D_i{}'}{R_i^2}$
10	0.006456	0.001298	0.006766	0.002214
20	0.003905	0.001232	0.004035	0.001352
30	0.00364	0.001109	0.003936	0.001093
40	0.004434	0.000918	0.004309	0.000843
50	0.003626	0.000668	0.003848	0.000647
	AC3-5(45°C)		AC3-5(60°C)	
	$\frac{D_a{}'}{R_a^2}$	$\frac{D_i{}'}{R_i^2}$	$\frac{D_a{}'}{R_a^2}$	$\frac{D_i{}'}{R_i^2}$
10	0.00474	0.001204	0.006154	0.001219
20	0.004236	0.001084	0.005713	0.001271
30	0.002956	0.000681	0.003323	0.000688
40	0.003802	0.000976	0.002843	0.000681
50	0.002828	0.000815	0.002893	0.000669

As the macropore effective diffusivity is much larger than the micropore effective diffusivity, the $\frac{D_a{}'}{R_a^2}$ is compared between all the shale samples. Fig 5 shows that TOC has a weak positive relation with $\frac{D_a{}'}{R_a^2}$ at 10bar, while a strong positive relation exists between the $\frac{D_a{}'}{R_a^2}$ at 10bar and micropore volume. This phenomenon demonstrates that the contribution of micropore volume to the macropore effective diffusivity is more significant than the TOC. Sample AC3-2 with low TOC but large micropore volume has a great macropore effective diffusivity. It might be implied that the larger micropore volume offers more available void space for gas diffusion. However, the sum of mesopore and macropore (<100nm) volume shows no relation with the $\frac{D_a{}'}{R_a^2}$ at 10 and 50bar (Figure 6), indicating the pores in the range of 2 to 100nm have little contribution to the macropore effective diffusivity. Therefore, the diffusion at low pressure in shale is mainly controlled by micropores rather than mesopores and macropores.

Herein, a hypothetic pore model is proposed in Figure 7. Pores in shale plays different roles in gas transport and storage: micropore connected with mesopore or macropore dominates the diffusion as a throat; mesopore or macropore is related to gas storage but not diffusion. The hypothetic pore model in shale could explain the different relations of the macropore effective diffusivity to the micropore volume and the sum of mesopore and macropore (<100nm) volume, but more investigates are necessary to verify the model.

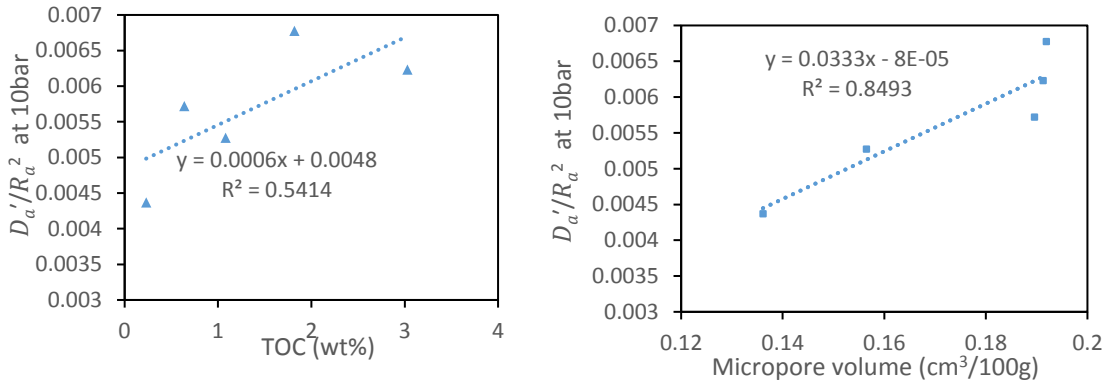

Figure 5 The relation of $\frac{D_a{}'}{R_a^2}$ at 10bar to the TOC and micropore volume for the shale samples.

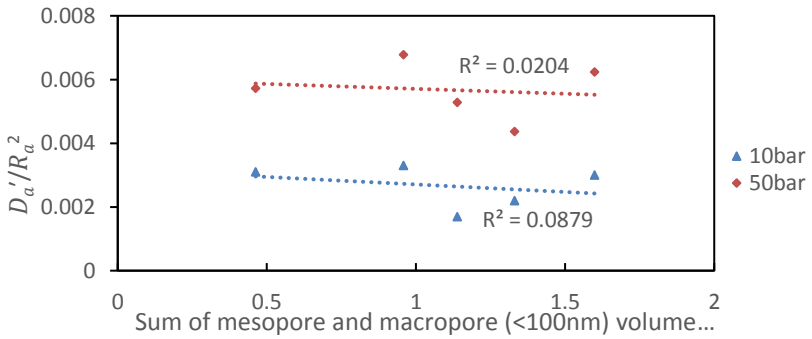

Figure 6 The relations of $\frac{D_a{}'}{R_a^2}$ at 10 and 50bar to the sum of mesopore and macropore (<100nm) volume

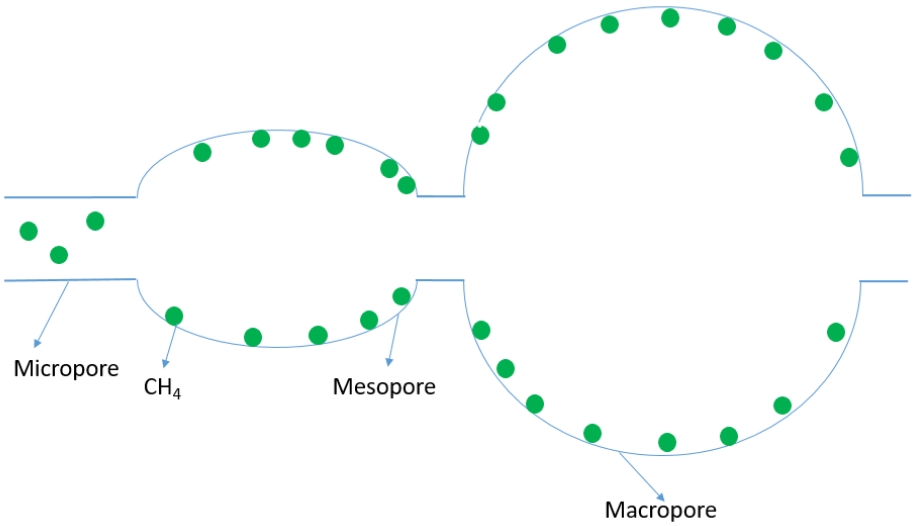

Figure 7 A hypothetic pore model in shale: micropore plays the role of throat and contributes to the diffusion.

It is worth mentioning that macropore and micropore diffusivity are not discussed in this study. For the determination of the macropore and micropore diffusivity in bidisperse model, pore structure parameters are needed to know, including porosity and specific surface area for both micropore and macropore. However, these parameters are unobtainable, as it is hard to distinguish the micropore and macropore precisely.

Conclusion

The methane adsorption kinetics and diffusion of 5 shale samples from Perth basin in Western Australia were studied. The methane adsorption rate was measured by experiment and the effective diffusivities were fitted using the bidisperse diffusion model. The major conclusions are as follows:

- Pressure has negative effect on methane adsorption rate, while temperature can positively affect the adsorption rate. TOC shows a positive relation with methane adsorption rate at high pressure (50bar) and the micropore volume is positively related to the methane adsorption rate at 30 bar.
- The pressure effect on the macropore and micropore diffusivity is negative, while the temperature effect on the macropore effective diffusivity is positive. In addition, the temperature effect on the micropore effective diffusivity is very limited.
- The relation between TOC and the macropore effective diffusivity at low pressure (10bar) is positive but weak, while micropore volume from low-pressure CO_2 adsorption displays a good positive relation with the macropore effective diffusivity at low pressure (10bar). However, no relation was found between the sum volume of mesopores and macropores (<100nm) and the macropore effective diffusivity.
- A hypothetic pore model is proposed to explain the effect of pores on diffusion in shale: micropore controls the effective diffusivity as a throat, while mesopore or macropore (<100nm) has limited contribution to the diffusion but gas storage.
- This findings highlight that the micropores in shales need to be redefined as pore throats that connects pores rather than pore itself.

Acknowledgments

The authors would like to thank China Scholarship Council (File No.201506440050) for providing financial assistance.

References

Bhowmik, S. and Dutta, P., 2013. Adsorption rate characteristics of methane and CO2 in coal samples from Raniganj and Jharia coalfields of India. International Journal of Coal Geology, 113: 50-59.

Brunauer, S., Emmett, P.H. and Teller, E., 1938. Adsorption of Gases in Multimolecular Layers. Journal of the American Chemical Society, 60: 309.

Busch, A., Gensterblum, Y., Krooss, B.M. and Littke, R., 2004. Methane and carbon dioxide adsorption–diffusion experiments on coal: upscaling and modeling. International Journal of Coal Geology, 60(2): 151-168.

Bustin, A.M.M. and Bustin, R.M., 2012. Importance of rock properties on the producibility of gas shales. International Journal of Coal Geology, 103: 132-147.

Chalmers, G.R. and Bustin, M.R., 2010. PS The Effects and Distribution of Moisture in Gas Shale Reservoir Systems.

Chalmers, G.R.L. and Bustin, R.M., 2007. The organic matter distribution and methane capacity of the Lower Cretaceous strata of Northeastern British Columbia, Canada. International Journal of Coal Geology, 70(1–3): 223-239.

Chen, M. et al., 2018. Methane diffusion in shales with multiple pore sizes at supercritical conditions. Chemical Engineering Journal, 334: 1455-1465.

Clarkson, C.R. and Bustin, R.M., 1999. The effect of pore structure and gas pressure upon the transport properties of coal: a laboratory and modeling study. 1. Isotherms and pore volume distributions. Fuel, 78(11): 1333-1344.

CUI, X., BUSTIN, A.M.M. and BUSTIN, R.M., 2009. Measurements of gas permeability and diffusivity of tight reservoir rocks: different approaches and their applications. Geofluids, 9(3): 208-223.

Cui, X., Bustin, R.M. and Dipple, G., 2004. Selective transport of CO2, CH4, and N2 in coals: insights from modeling of experimental gas adsorption data. Fuel, 83(3): 293-303.

Curtis, J.B., 2002. Fractured Shale-Gas Systems. AAPG Bulletin, 86(11): 1921-1938.

Dang, W. et al., 2017. Methane Adsorption Rate and Diffusion Characteristics in Marine Shale Samples from Yangtze Platform, South China, 10.

Gasparik, M. et al., 2014. Geological controls on the methane storage capacity in organic-rich shales. International Journal of Coal Geology, 123: 34-51.

Greenspan, L., 1977. Humidity fixed points of binary saturated aqueous solutions. Journal of research of the national bureau of standards, 81(1): 89-96.

Guo, S., 2013. Experimental study on isothermal adsorption of methane gas on three shale samples from Upper Paleozoic strata of the Ordos Basin. Journal of Petroleum Science and Engineering, 110: 132-138.

Ji, L., Zhang, T., Milliken, K.L., Qu, J. and Zhang, X., 2012. Experimental investigation of main controls to methane adsorption in clay-rich rocks. Applied Geochemistry, 27(12): 2533-2545.

Kuila, U. et al., 2014. Nano-scale texture and porosity of organic matter and clay minerals in organic-rich mudrocks. Fuel, 135(Supplement C): 359-373.

Labani, M.M., Rezaee, R., Saeedi, A. and Hinai, A.A., 2013. Evaluation of pore size spectrum of gas shale reservoirs using low pressure nitrogen adsorption, gas expansion and

mercury porosimetry: A case study from the Perth and Canning Basins, Western Australia. Journal of Petroleum Science and Engineering, 112: 7-16.
Li, Z.-Z., Min, T., Kang, Q., He, Y.-L. and Tao, W.-Q., 2016. Investigation of methane adsorption and its effect on gas transport in shale matrix through microscale and mesoscale simulations. International Journal of Heat and Mass Transfer, 98: 675-686.
Liu, K., Ostadhassan, M., Zhou, J., Gentzis, T. and Rezaee, R., 2017. Nanoscale pore structure characterization of the Bakken shale in the USA. Fuel, 209: 567-578.
Mianowski, A. and Marecka, A., 2009. The isokinetic effect as related to the activation energy for the gases diffusion in coal at ambient temperatures. Journal of Thermal Analysis and Calorimetry, 96(2): 495-499.
Rani, S., Prusty, B.K. and Pal, S.K., 2018. Adsorption kinetics and diffusion modeling of CH4 and CO2 in Indian shales. Fuel, 216: 61-70.
Ravikovitch, P.I., Haller, G.L. and Neimark, A.V., 1998. Density functional theory model for calculating pore size distributions: pore structure of nanoporous catalysts. Advances in Colloid and Interface Science, 76-77(Supplement C): 203-226.
Ross, D.J.K. and Marc Bustin, R., 2007. Shale Gas Potential of the Lower Jurassic Gordondale Member, Northeastern British Columbia, Canada. CSPG Bulletin, 55(1): 25.
Ross, D.J.K. and Marc Bustin, R., 2009. The importance of shale composition and pore structure upon gas storage potential of shale gas reservoirs. Marine and Petroleum Geology, 26(6): 916-927.
Rouquerol, J. et al., 1994. Recommendations for the characterization of porous solids (Technical Report), Pure and Applied Chemistry, pp. 1739.
Ruckenstein, E., Vaidyanathan, A.S. and Youngquist, G.R., 1971. Sorption by solids with bidisperse pore structures. Chemical Engineering Science, 26(9): 1305-1318.
Siemieniewska, T. et al., 1990. Application of the Dubinin-Astakhov equation to evaluation of benzene and cyclohexane adsorption isotherms on steam-gasified humic acid chars from brown coal. Energy & Fuels, 4(1): 61-70.
Wang, J. et al., 2016. Measurement of dynamic adsorption–diffusion process of methane in shale. Fuel, 172: 37-48.
Wang, L. and Yu, Q., 2016. The effect of moisture on the methane adsorption capacity of shales: A study case in the eastern Qaidam Basin in China. Journal of Hydrology, 542: 487-505.
Yuan, W. et al., 2014. Experimental study and modelling of methane adsorption and diffusion in shale. Fuel, 117: 509-519.
Zhang, T., Ellis, G.S., Ruppel, S.C., Milliken, K. and Yang, R., 2012. Effect of organic-matter type and thermal maturity on methane adsorption in shale-gas systems. Organic Geochemistry, 47: 120-131.
Zou, J., Rezaee, R. and Liu, K., 2017. The effect of temperature on methane adsorption in shale gas reservoirs. Energy & Fuels.